Tuijin Jishu/Journal of Propulsion Technology
ISSN: 1001-4055
Vol. 47 No. 01(2026)

Heat Source and Slip Impacts on Porous Medium Flow of Williamson Nanofluid: Numerical Approach via Keller-Box Scheme

Archie Thakur [1],
[1]*Department of Mathematics, CMR Institute of Technology, Bengaluru, Karnataka, India. Pin Code: 560037*
archiethakur93@gmail.com

Abstract: This study presents a mathematical model to analyze the combined effects of prescribed heat sources, velocity slip, and thermal slip on the stagnation point boundary layer flow of a non-Newtonian Williamson nanofluid. The investigation incorporates a time-varying magnetic field and considers two thermal boundary conditions—prescribed surface temperature and prescribed heat flux—within the framework of the Buongiorno nanofluid model. To account for fluid movement through porous media, the Darcy–Forchheimer model is employed. Using similarity transformations, the governing partial differential equations are reduced to a set of nonlinear ordinary differential equations. These equations are then numerically solved using the Keller-box method, an implicit finite difference approach well-suited for handling nonlinear boundary value problems. Numerical results for velocity, temperature, and concentration profiles are illustrated through 2D plots, while 3D visualizations highlight the influence of various parameters on the skin friction coefficient, Nusselt number, and Sherwood number. The findings contribute to a deeper understanding of Williamson nanofluid dynamics in porous environments and hold potential applications in the optimization of nanofluid-based thermal systems.

Keywords Williamson nanofluid, Darcy-Forchheimer model, slip effects, MHD, Mixed convection, Stagnated flow, PST, PHF, Keller-Box scheme.

1 Introduction

Owing to their unique flow characteristics, non-Newtonian fluids have become a focus of extensive investigation, especially due to their relevance in a variety of industrial processes, including those in the chemical sector, biomedical devices, and mechanical systems [40]. Their usage extends to numerous physical processes such as the fabrication of glass fibers, the production of adhesive tapes, and the drawing of paper films [10]. To characterize the complex rheological behavior of these fluids—exemplified by materials like honey, paint, and toothpaste—several mathematical models have been proposed, including the Cross, Power-law, Ellis, Carreau, and Casson nanofluid models. Among these, the Williamson model, introduced in 1929 [46], provides a nonlinear framework capable of capturing the flow dynamics of pseudoplastic fluids through appropriate mathematical formulations. A broad range of research

has employed the Williamson nanofluid model to explore flow and heat transfer phenomena in non-Newtonian media [32], [2], [7], [21], [47], [6], [36], [23], [15], [18]. A pioneering study by Nadeem and Hussain [33] presented the initial analysis of heat transfer characteristics in Williamson nanofluids. Subsequently, Khan and Khan [20] investigated the boundary layer behavior of such fluids using the Homotopy Analysis Method (HAM). Building on this, Kho et al. [19] examined the combined effects of velocity and thermal slip on heat and mass transfer in Williamson nanofluid flow. Recent advancements in the thermal analysis of these fluids are well-documented in studies such as [13], [11], [41], [24], [25], reflecting the growing importance of the Williamson model in modern fluid dynamics research.

A porous medium consists of a solid matrix with interconnected voids, characterized by porosity (void fraction) and permeability (fluid flow capability) [3], [29]. While porosity indicates a material's fluid retention capacity, permeability defines how easily fluid flows through it. Thermally induced convection in porous media finds applications in insulation, underground waste disposal, food processing, metallurgy, and microelectronics. Attia [4] examined stagnation flow over a permeable surface and found that increasing porosity reduces boundary layer thickness and increases wall shear stress. Mohammed and Dawood [30] studied unsteady mixed convection in saturated porous media using the Brinkman–Forchheimer model. Darcy's law laid the foundation for modeling fluid flow through porous media, particularly under low permeability and velocity conditions. However, it fails to account for inertial and boundary effects at higher porosities and flow rates [45]. To address this, Forchheimer introduced a nonlinear correction involving a velocity-squared term [27], [38], [5], [17]. Pal and Mondal [37] explored boundary layer flow over a vertically stretching sheet in non-Darcy porous media. Ganesh et al. [8] analyzed nanofluid flow with second-order slip, Ohmic heating, and viscous dissipation using the Darcy–Forchheimer model over a stretching surface. Similarly, Kumar et al. [22] applied the same model to study 3D stagnation flow of Casson fluid.

In scenarios where the no-slip boundary condition fails, partial slip conditions—where fluid velocity at the boundary is non-zero—must be considered [44]. Slip flow arises when fluid near the surface moves at a different velocity than the boundary itself. The *slip length* L_s quantifies this behavior, defined as the extrapolated distance beneath the surface where tangential velocity becomes zero. The corresponding slip velocity is given by $V_s = L_s \frac{\partial u}{\partial y}$, and is influenced by factors such as shear stress, surface roughness, and fluid viscosity. Although the no-slip condition is a cornerstone of classical boundary layer theory, partial slip conditions often provide a more accurate representation of real-world applications in engineering and industry. The presence of nanoparticles has been identified as a contributing factor to velocity slip at boundaries [9]. Additional causes include contact with lubricated or porous surfaces [43]. Recent studies have explored these effects: Noghrehabadi et al. [35] analyzed slip behavior with varying nanoparticle concentrations over a stretching surface, while Mukhopadhyay [31] solved for boundary layer flow with slip using the shooting method. Ibrahim and Shankar [42] examined nanofluid flow

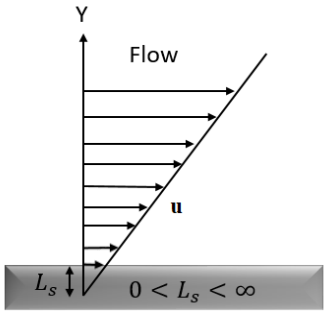

Figure a: Partial slip boundary condition.

with velocity, thermal, and solutal slip over a permeable stretching sheet. Similarly, Malvandi et al. [28] and Ramya et al. [39] investigated combined slip effects on unsteady and nonlinear stretching flows of nanofluids

This study aims to model and analyze the combined influence of unsteadiness, magnetic field, mixed convection, and slip conditions on the stagnation point flow of Williamson nanofluid over a linearly stretching sheet embedded in a porous medium. The Darcy–Forchheimer model is employed, considering two thermal boundary conditions: prescribed surface temperature (PST) and prescribed heat flux (PHF). This work extends the study by Thakur and Sood [3], which investigated MHD mixed convection of Williamson nanofluid under PST and PHF using MATLAB's bvp4c solver. In contrast, the present analysis adopts the Keller-box method and incorporates slip effects, adding a novel dimension to the problem.

2 Analytical framework of the study

This study examines unsteady, two-dimensional mixed convection and stagnation point flow of a Williamson nanofluid over a linearly stretching surface in a porous medium, incorporating slip boundary conditions. As shown in Figure 2, the sheet stretches bidirectionally along the x-axis from $t = 0$, with flow developing in the y-direction. A magnetic field of strength $\frac{B_0}{\sqrt{1-\gamma t}}$ is applied along the y-axis in the region $y > 0$. The surface and free stream velocities are defined as $U_w(x) = \frac{ax}{1-\gamma t}$ and $U_\infty(x) = \frac{bx}{1-\gamma t}$, where $a > 0$ and $b \geq 0$ are stretching and stagnation parameters, respectively. Both velocities vary with x, indicating spatial dependence from the stagnation point. External and induced electric fields are neglected.

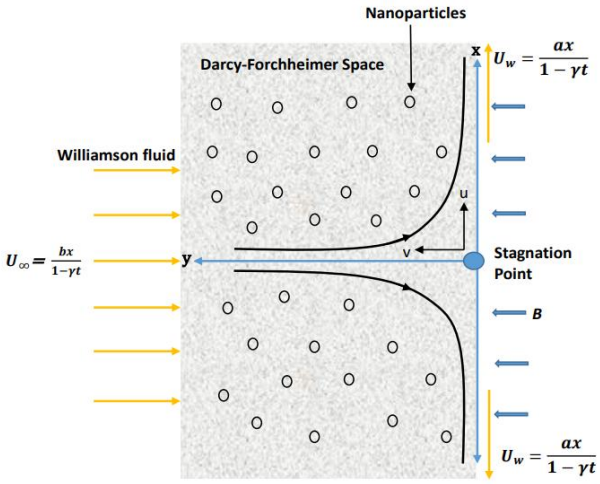

Figure b: Schematic representation of the system.

2.1 Governing Equations

In Cartesian coordinate systems, the flow behavior is characterized by a set of partial differential equations, incorporating the Boussinesq approximation, as follows (see [12], [1], & [16]):

$$\frac{\partial u}{\partial x} + \frac{\partial v}{\partial y} = 0, \tag{1}$$

$$\frac{\partial u}{\partial t} + u\frac{\partial u}{\partial x} + v\frac{\partial u}{\partial y} = \frac{dU_\infty}{dt} + U_\infty \frac{dU_\infty}{dx} + \nu\frac{\partial^2 u}{\partial y^2} + \sqrt{2}\nu\Gamma\frac{\partial u}{\partial y}\frac{\partial^2 u}{\partial y^2} + \frac{\nu}{k^*}(U_\infty - u) + F({U_\infty}^2 - u^2) +$$

$$\sigma\frac{B^2}{\rho}(U_\infty - u) + g\beta_T(T - T_\infty) + g\beta_C(C - C_\infty), \tag{2}$$

$$\frac{\partial C}{\partial t} + u\frac{\partial C}{\partial x} + v\frac{\partial C}{\partial y} = D_B\frac{\partial^2 C}{\partial y^2} + \frac{D_T}{T_\infty}\frac{\partial^2 T}{\partial y^2}, \tag{3}$$

with dominated boundary conditions,

$$\begin{aligned} u &= U_w + \xi_1 v_f\frac{\partial u}{\partial y} = \frac{ax}{1-\gamma t} + \xi_1\frac{\partial u}{\partial y}, \quad v = 0, \quad C = C_w = C_\infty + \frac{Ax}{1-\gamma t} && at \quad y = 0, \\ u &= U_\infty = \frac{bx}{1-\gamma t}, \quad C \to C_\infty && as \quad y \to \infty, \end{aligned} \tag{4}$$

where $\nu = \frac{\mu}{\rho}$, $B = \frac{B_0}{\sqrt{1-\gamma t}}$, $k^* = k_0(1-\gamma t)$, $\gamma t < 1$, here k_0 is a constant which gives initial permeability, γ and A are positive constants (s^{-1}), T_∞ is ambient fluid temperature, C_∞ is ambient fluid concentration, $F = \frac{C_b}{x\sqrt{k^*}}$ characterizes the non-uniform inertia coefficient of the porous medium, g is acceleration due to gravity, β_T and β_C are thermal and concentration expansion coefficient and ξ_1 is the velocity slip length.

2.2 Similarity transformations

The following similarity transformations, adapted from the approach in Majeed et al. [?], are applied:

$$\psi = \sqrt{\frac{a\nu}{1-\gamma t}}xf(\eta), \quad \eta = \sqrt{\frac{a}{\nu(1-\gamma t)}}y, \quad \phi(\eta) = \frac{C - C_\infty}{C_w - C_\infty}. \tag{5}$$

Here, ψ denotes the stream function, satisfying $u = \frac{\partial\psi}{\partial y}$ and $v = -\frac{\partial\psi}{\partial x}$. The quantity C_w represents the wall concentration, while f and ϕ are expressed as functions of the similarity variable η.

Eq. (1) is being identically verified while considering eq. (5), rest of the eqs. (2) & (3) are transformed as,

$$\begin{aligned} &f''' + ff'' + Wef''f''' - f'^2 + \epsilon^2 + (M+\lambda)(\epsilon - f') + Fr(\epsilon^2 - f'^2) \\ &-\beta\left(\frac{\eta}{2}f'' + f' - \epsilon\right) + G(\theta + N\phi) = 0, \end{aligned} \tag{6}$$

$$\phi'' - Sc\left[\beta\left(\left(\frac{\eta}{2}\phi' + \phi\right) + f'\phi - f\phi'\right)\right] + \frac{1}{N_{bt}}\theta'' = 0, \tag{7}$$

where, the prime symbol ($'$) indicates differentiation with respect to the similarity variable η, and the dimensionless parameters are defined as follows:

$$We = \Gamma x\sqrt{\frac{2a^3}{\nu(1-\gamma t)^3}},\quad Fr = \frac{C_b}{\sqrt{k^*}},\quad M = \frac{\sigma B_0^2}{\rho a},\quad \lambda = \frac{\nu}{k_0 a},\quad G = \frac{Gr_x}{Re_x{}^2},\quad \beta = \frac{\gamma}{a}$$

$$N = \frac{\beta_C(C_w - C_\infty)}{\beta_T(T_w - T_\infty)},\quad N_{bt} = \frac{T_\infty D_B(C_w - C_\infty)}{D_T(T_w - T_\infty)},\quad Sc = \frac{\nu}{D_B},\quad \epsilon = \frac{b}{a}\quad and\quad Gr_x = \frac{g\beta_T(T_w - T_\infty)x^3}{\nu^2}$$

The resulting boundary conditions in terms of similarity variables (5) are:

$$\begin{aligned} f(\eta) &= 0,\quad f'(\eta) - S_1 f''(\eta) = 1,\quad \phi(\eta) = 1 \quad at \quad \eta = 0, \\ f'(\eta) &= \epsilon,\quad \phi(\eta) = 0 \quad as \quad \eta \to \infty. \end{aligned} \tag{8}$$

Here, $S_1 = \xi_1\sqrt{\frac{a}{\nu(1-\gamma t)}}$ is the velocity slip parameter.

3 Evaluation of Heat Propagation Behavior

The thermal energy equation for the system is formulated as:

$$\frac{\partial T}{\partial t} + u\frac{\partial T}{\partial x} + v\frac{\partial T}{\partial y} = \alpha\frac{\partial^2 T}{\partial y^2} + \frac{\rho_p C_p}{\rho C}\left[D_B\frac{\partial C}{\partial y}\frac{\partial T}{\partial y} + \frac{D_T}{T_\infty}\left(\frac{\partial T}{\partial y}\right)^2\right], \tag{9}$$

where $\alpha = \frac{k}{\rho C}, \rho C$ and $\rho_p C_p$ characterizes heat capacity of nanofluid and heat capacity of nanoparticles respectively. The thermal analysis is carried out for two distinct heat transfer cases:

3.1 Governing equations for the PST case

In this case, the boundary conditions are:

$$\begin{aligned} T &= T_w + \xi_2\frac{\partial T}{\partial y} = T_\infty + \frac{Sx}{1-\gamma t} + \xi_2\frac{\partial T}{\partial y} \quad at \quad y = 0, \\ T &\to T_\infty \quad as \quad y \to \infty. \end{aligned} \tag{10}$$

Here S is a positive constant. $S = 0$ corresponds to forced convection limit i.e. an absence of buoyancy force whereas $S > 0$ and $S < 0$ represent assisting and opposing flows respectively. According to the imposed similarity transformations, the non-dimensional temperature $\theta(\eta)$ is defined as:

$$\theta(\eta) = \frac{T - T_\infty}{T_w - T_\infty}. \tag{11}$$

Here, T_w is the temperature at the wall.

While considering eq. (11), eq. (9) is transformed as:

$$\theta'' - Pr\left[\beta\left(\frac{\eta}{2}\theta' + \theta\right) + f'\theta - f\theta'\right] + \frac{N_c}{Le}\phi'\theta' + \frac{N_c}{LeN_{bt}}\theta'^2 = 0, \tag{12}$$

where, the prime symbol ($'$) denotes derivatives with respect to η, and the dimensionless parameters are specified as:

$$Pr = \frac{\nu}{\alpha}, \quad N_c = \frac{\rho_p C_p}{(\rho C)}(C_w - C_\infty),$$

$$N_{bt} = \frac{T_\infty D_B (C_w - C_\infty)}{D_T (T_w - T_\infty)}, \quad Le = \frac{\alpha}{D_B}.$$

The resulting boundary conditions in terms of similarity variables are:

$$\begin{aligned} &\theta(\eta) - S_2\theta'(\eta) = 1 \qquad at \quad \eta = 0, \\ &\theta(\eta) = 0 \qquad\qquad\quad as \quad \eta \to \infty. \end{aligned} \tag{13}$$

Here, $S_2 = \xi_2\sqrt{\frac{a}{\nu(1-\gamma t)}}$ is the thermal slip parameter.

3.2 Governing equations for the PHF case

In this case, the boundary conditions are:

$$\begin{aligned} &-\kappa\frac{\partial T}{\partial y} = q_w = T_\infty + \frac{Dx}{1-\gamma t} \qquad at \quad y = 0, \\ &T \to T_\infty \qquad\qquad\qquad\qquad as \quad y \to \infty. \end{aligned} \tag{14}$$

Defining $T = \frac{Dx}{\kappa(1-\gamma t)}\sqrt{\frac{\nu(1-\gamma t)}{a}}h(\eta) + T_\infty$.

Here, q_w represents the rate of heat transfer and D is a positive constant.

According to the imposed similarity transformations, the non-dimensional scaled temperature $\Theta(\eta)$ is defined as:

$$\Theta(\eta) = \frac{T - T_\infty}{T_w - T_\infty}. \tag{15}$$

While considering eq. (15), eq. (9) is transformed as:

$$\Theta'' - Pr\left[\frac{\beta}{2}(\eta\Theta' + \Theta) + f'\Theta - f\Theta'\right] + \frac{N_c}{Le}\phi'\Theta' + \frac{N_c}{LeN_{bt}}\Theta'^2 = 0, \tag{16}$$

where, the prime symbol ($'$) denotes derivatives with respect to η, and the dimensionless parameters are specified as:

$$Pr = \frac{\nu}{\alpha}, \quad N_c = \frac{\rho_p C_p}{(\rho C)}(C_w - C_\infty),$$

$$N_{bt} = \frac{T_\infty D_B (C_w - C_\infty)}{D_T (T_w - T_\infty)}, \quad Le = \frac{\alpha}{D_B}.$$

The resulting boundary conditions in terms of similarity variables are:

$$\begin{aligned} \Theta'(\eta) &= -1 \quad at \quad \eta = 0, \\ \Theta(\eta) &= 0 \quad as \quad \eta \to \infty. \end{aligned} \tag{17}$$

4 Parameters of empirical importance

Skin-friction coefficient, local Nusselt number, and Sherwood number are specified to be:

$$C_f = \frac{\tau_w}{\rho U_w{}^2(x)}, \quad Nu = \frac{x q_w}{\kappa (T_w - T_\infty)}, \quad Sh = \frac{x q_m}{D_B (C_w - C_\infty)},$$

where τ_w is used for the shear stress of Williamson nanofluid at the surface of the wall, q_w gives the heat flux from the wall, and q_m gives the mass flux of the nanoparticle volume fraction from the wall. These terms are given as:

$$\tau_w = \mu \left[\frac{\partial u}{\partial y} + \frac{\Gamma}{\sqrt{2}} \left(\frac{\partial u}{\partial y} \right)^2 \right]_{y=0}, \quad q_w = -\kappa \left(\frac{\partial T}{\partial y} \right)_{y=0}, \quad \text{and} \quad q_m = -D_B \left(\frac{\partial C}{\partial y} \right)_{y=0}.$$

Upon imposing the similarity transformations and dominated boundary conditions, the non-dimensional forms of skin friction coefficient, local Nusselt number, and Sherwood number are specified as:

$$C_{fx} = C_f (Re)^{\frac{1}{2}} = \left(f''(\eta) + \frac{We}{2} f''(\eta)^2 \right)_{\eta=0},$$

$$Nu_x = Nu (Re)^{-\frac{1}{2}} = \begin{cases} (-\theta'(\eta))_{\eta=0}, & \text{PSTCase}, \\ \left(\frac{1}{\Theta(\eta)} \right)_{\eta=0}, & \text{PHFCase}, \end{cases}$$

$$Sh_x = Sh (Re)^{-\frac{1}{2}} = (-\phi'(\eta))_{\eta=0},$$

where $Re = \frac{U_w(x)}{\nu(1-\gamma t)} x$ is the Reynold's number.

5 Execution of the Keller Box Scheme

Keller-box method is one such scheme which is capable of giving numerical solutions to non-linear cases over some fixed region in the province of the problem. Keller-box method is an implicit finite difference scheme advanced by Cebeci and Bradshaw in 1984 which is very

popular because of its accuracy and convergence. To obtain the solution utilizing Keller-Box method comprises of the following steps:

- First, we reduce the system of non-linear differential equations into a system of first order differential equation
- We further substitute the functions by mean values and their derivatives with central difference formulas and as a result we will get a system of non-linear algebraic difference equations where the number of unknowns is equal to the number of difference equations and boundary conditions.
- Then we use Newton's linearization technique to linearize the non-linear terms in the difference equations. (if they are non linear).
- Lastly, Block tri-diagonal scheme is used to solve the resultant system.

Transformation to first order system

To write equations in first order system, we have to introduce new dependent variable m, n, q, s such that

$$f' = m, \quad m' = n, \quad \theta' = q\ (PST), \quad \Theta' = q\ (PHF) \quad \phi' = s, \tag{18}$$

where $(')$ shows the differentiation with η. Therefore, equations can be written as:

$$n' + Wennn' + fn - m^2 + \epsilon^2 - \beta\left(\frac{\eta}{2}n + m - \epsilon\right) + (M + \lambda)(\epsilon - m) + Fr(\epsilon^2 - m^2) + G(\theta + N\phi) = 0, \tag{19}$$

$$q' + \frac{N_c}{Le}sq + \frac{N_c}{LeN_{bt}}q^2 - Pr\left[\beta\left(\frac{\eta}{2}q + \theta\right) + m\theta - fq\right] = 0, (PST) \tag{20}$$

$$q' + \frac{N_c}{Le}sq + \frac{N_c}{LeN_{bt}}q^2 - Pr\left[\frac{\beta}{2}(\eta q + h) + uh - fq\right] = 0, (PHF) \tag{21}$$

$$s' - Sc\left[\beta\left(\frac{\eta}{2}s + \phi\right) + u\phi - fs\right] + \frac{1}{N_{bt}}q' = 0. \tag{22}$$

The boundary conditions are formed as:

Prescribed surface temperature

$$\left.\begin{array}{llll} f = 0, & m = 1, & \theta = 1, & \phi = 1, \quad at \quad \eta = 0, \\ m = \epsilon, & \theta = 0, & \phi = 0, & as \quad \eta \to \infty. \end{array}\right\} \tag{23}$$

Prescribed heat flux

$$\left.\begin{array}{llll} f = 0, & m = 1, & q = -1, & \phi = 1, \quad at \quad \eta = 0, \\ m = \epsilon, & \Theta = 0, & \phi = 0, & as \quad \eta \to \infty. \end{array}\right\} \tag{24}$$

Finite difference scheme

Now the finite difference approximation to equations (18-22) produce the following set of equations :

$$f_j - f_{j-1} - h_j(m_j + m_{j-1})/2 = 0, \quad (25)$$
$$m_j - m_{j-1} - h_j(n_j + n_{j-1})/2 = 0, \quad (26)$$
$$\theta_j - \theta_{j-1} - h_j(q_j + q_{j-1})/2 = 0, (PST) \quad (27)$$
$$\Theta_j - \Theta_{j-1} - h_j(q_j + q_{j-1})/2 = 0, (PHF) \quad (28)$$
$$\phi_j - \phi_{j-1} - h_j(s_j + s_{j-1})/2 = 0, \quad (29)$$

$$n_j - n_{j-1} + \frac{We}{2}(n_j + n_{j-1})(n_j - n_{j-1}) + \frac{h_j}{4}(f_j + f_{j-1})(n_j + n_{j-1}) - \frac{h_j}{4}(m_j + m_{j-1})^2$$
$$-\beta h_j\left(\frac{\eta}{4}(n_j + n_{j-1}) + \frac{1}{2}(m_j + m_{j-1}) - \epsilon\right) + (M + \lambda)\frac{h_j}{2}\left(2\epsilon - (m_j + m_{j-1})\right) +$$
$$Fr\frac{h_j}{4}\left(4\epsilon^2 - (m_j + m_{j-1})^2\right) + G\frac{h_j}{2}\left(\theta_j + \theta_{j-1} + N(\phi_j + \phi_{j-1})\right) = 0, \quad (30)$$

$$q_j - q_{j-1} + \frac{N_c}{Le}\frac{h_j}{4}(s_j + s_{j-1})(q_j + q_{j-1}) + \frac{N_c}{LeN_{bt}}\frac{h_j}{4}(q_j + q_{j-1})^2 - h_j Pr(\beta$$
$$+\frac{1}{2}(\theta_j + \theta_{j-1})) + \frac{1}{4}(m_j + m_{j-1})(\theta_j + \theta_{j-1}) - \frac{1}{4}(f_j + f_{j-1})(q_j + q_{j-1})) = 0, \quad (31)$$

$$q_j - q_{j-1} + \frac{N_c}{Le}\frac{h_j}{4}(s_j + s_{j-1})(q_j + q_{j-1}) + \frac{N_c}{LeN_{bt}}\frac{h_j}{4}(q_j + q_{j-1})^2 - h_j Pr\frac{\beta}{2}$$
$$+\frac{1}{2}(\Theta_j + \Theta_{j-1})) + \frac{1}{4}(m_j + m_{j-1})(\Theta_j + \Theta_{j-1}) - \frac{1}{4}(f_j + f_{j-1})(q_j + q_{j-1})) = 0, \quad (32)$$

$$s_j - s_{j-1} - h_j Sc(\beta\left(\frac{\eta}{4}(s_j + s_{j-1}) + \frac{1}{2}(\phi_j + \phi_{j-1})\right) + \frac{1}{4}(m_j + m_{j-1})(\theta_j + \theta_{j-1})$$
$$-\frac{1}{4}(f_j + f_{j-1})(s_j + s_{j-1})) + \frac{1}{N_{bt}}(q_j - q_{j-1}) = 0. \quad (33)$$

These equations are inflicted for $j = 1,2,3,\ldots,J-1$ and at $j = 0$, $j = J$, the boundary conditions for both prescribed heat sources (PST and PHF) are respectively:

$$f_0 = 0, \quad m_0 = 1, \quad \theta_0 = 1, \quad \phi_0 = 1, \quad m_J = \epsilon, \quad \theta_J = 0, \quad \phi_J = 0.\} \quad (34)$$

$$f_0 = 0, \quad m_0 = 1, \quad q_0 = -1, \quad \phi_0 = 1, \quad m_J = \epsilon, \quad \Theta_J = 0, \quad \phi_J = 0.\} \quad (35)$$

Newton's linearization method

To solve these non-linear equations (25 - 33), we have employed Newton's method. For that we

have introduced following iterates $[\ f_j^i, m_j^i, n_j^i, \theta_j^i(PST), \Theta_j^i(PHF), q_j^i, \phi_j^i, s_j^i\ ]$, where $i = 0,1,2,\ldots..$ For the higher iterates, we set:

$$\begin{aligned}
f_j^{i+1} &= f_j^i + \delta f_j^i, & m_j^{i+1} &= m_j^i + \delta m_j^i, & n_j^{i+1} &= n_j^i + \delta v_j^i,\\
\theta_j^{i+1} &= \theta_j^i + \delta\theta_j^i\ (PST), & q_j^{i+1} &= q_j^i + \delta q_j^i, & \Theta_j^{i+1} &= \Theta_j^i + \delta\Theta_j^i\ (PHF),\\
\phi_j^{i+1} &= \phi_j^i + \delta\phi_j^i, & s_j^{i+1} &= s_j^i + \delta s_j^i.
\end{aligned} \tag{36}$$

Then we substituted the right-hand side of these equations in (25 - 33) and ignore the higher order terms in δ. Formulated linear equations are (drop superscript i for simplicity):

$$\left.\begin{aligned}
&\delta f_j - \delta f_{j-1} - h_j(\delta u_j + \delta u_{j-1})/2 &&= (r_1)_j,\\
&\delta m_j - \delta m_{j-1} - h_j(\delta n_j + \delta n_{j-1})/2 &&= (r_2)_j,\\
&\delta\theta_j - \delta\theta_{j-1} - h_j(\delta q_j + \delta q_{j-1})/2 &&= (r_3)_j,\\
&\delta\Theta_j - \delta\Theta_{j-1} - h_j(\delta q_j + \delta q_{j-1})/2 &&= (r_3)_j,\\
&\delta\phi_j - \delta\phi_{j-1} - h_j(\delta s_j + \delta s_{j-1})/2 &&= (r_4)_j,\\
&(a_1)_j\delta n_j + (a_2)_j\delta n_{j-1} + (a_3)_j\delta f_j + (a_4)_j\delta f_{j-1} + (a_5)_j\delta m_j + (a_6)_j\delta m_{j-1}\\
&+(a_7)_j\delta\theta_j + (a_8)_j\delta\theta_{j-1} + (a_9)_j\delta\phi_j + (a_{10})_j\delta\phi_{j-1} &&= (r_5)_j,\\
&(b_1)_j\delta q_j + (b_2)_j\delta q_{j-1} + (b_3)_j\delta f_j + (b_4)_j\delta f_{j-1} + (b_5)_j\delta m_j + (b_6)_j\delta m_{j-1}\\
&+(b_7)_j\delta\theta_j + (b_8)_j\delta\theta_{j-1} + (b_9)_j\delta s_j + (b_{10})_j\delta s_{j-1} &&= (r_6)_j,\\
&(b_1)_j\delta q_j + (b_2)_j\delta q_{j-1} + (b_3)_j\delta f_j + (b_4)_j\delta f_{j-1} + (b_5)_j\delta m_j + (b_6)_j\delta m_{j-1}\\
&+(b_7)_j\delta\Theta_j + (b_8)_j\delta\Theta_{j-1} + (b_9)_j\delta s_j + (b_{10})_j\delta s_{j-1} &&= (r_6)_j,\\
&(c_1)_j\delta s_j + (c_2)_j\delta s_{j-1} + (c_3)_j\delta f_j + (c_4)_j\delta f_{j-1} + (c_5)_j\delta m_j + (c_6)_j\delta m_{j-1}\\
&+(c_7)_j\delta\phi_j + (c_9)_j\delta\phi_{j-1} + (c_9)_j\delta q_j + (c_{10})_j\delta q_{j-1} &&= (r_7)_j.
\end{aligned}\right\} \tag{37}$$

where

$$(a_1)_j = 1 + Wen_j - \beta\frac{h_j}{4}\eta + \frac{h_j}{2}f_{j-\frac{1}{2}}, (a_2)_j = -1 - Wen_{j-1} - \beta\frac{h_j}{4}\eta + \frac{h_j}{2}f_{j-\frac{1}{2}},$$
$$(a_3)_j = \frac{h_j}{2}n_{j-\frac{1}{2}}, (a_4)_j = (a_3)_j,$$
$$(a_5)_j = -h_j m_{j-\frac{1}{2}} - \frac{h_j}{2}\beta - \frac{h_j}{2}(M+\lambda) - h_j Frm_{j-\frac{1}{2}}, (a_6)_j = (a_5)_j,$$
$$(a_7)_j = \frac{h_j}{2}G, (a_8)_j = (a_7)_j,$$
$$(a_9)_j = \frac{h_j}{2}GN, (a_{10})_j = (a_9)_j,$$

$$(b_1)_j = 1 + \frac{N_c}{Le}\frac{h_j}{2}s_{j-\frac{1}{2}} + \frac{N_c}{LeN_{bt}}h_j q_{j-\frac{1}{2}} - h_j Pr\left(\beta\frac{\eta}{4} - \frac{1}{2}f_{j-\frac{1}{2}}\right), (b_2)_j = (b_1)_j - 2,$$
$$(b_3)_j = Pr\frac{h_j}{2}q_{j-\frac{1}{2}}, (b_4)_j = (b_3)_j,$$
$$(b_5)_j = -Pr\frac{h_j}{2}\theta_{j-\frac{1}{2}}\ (PST), (b_6)_j = (b_5)_j,$$

$$(b_5)_j = -Pr\frac{h_j}{2}\Theta_{j-\frac{1}{2}}\ (PHF),$$
$$(b_7)_j = -Pr\frac{h_j}{2}(m_{j-\frac{1}{2}}+\beta)\ (PST), (b_8)_j = (b_7)_j,$$
$$(b_7)_j = -Pr\frac{h_j}{2}\left(m_{j-\frac{1}{2}}+\frac{1}{2}\beta\right)\ (PHF),$$
$$(b_9)_j = \frac{N_c}{Le}\frac{h_j}{2}q_{j-\frac{1}{2}}(b_{10})_j = (b_9)_j,$$
$$(c_1)_j = 1 - h_j Sc\left(\beta\frac{\eta}{4}-\frac{1}{2}f_{j-\frac{1}{2}}\right), (c_2)_j = (c_1)_j - 2,$$
$$(c_3)_j = Sc\frac{h_j}{2}s_{j-\frac{1}{2}}, (c_4)_j = (c_3)_j,$$
$$(c_5)_j = -Sc\frac{h_j}{2}s_{j-\frac{1}{2}}, (c_6)_j = (c_5)_j,$$
$$(c_7)_j = -Sc\frac{h_j}{2}(\beta + m_{j-\frac{1}{2}}), (c_8)_j = (c_7)_j,$$
$$(c_9)_j = \frac{1}{N_{bt}}, (c_{10})_j = -(c_9)_j.$$

$$(r_1)_j = f_{j-1} - f_j + h_j m_{j-\frac{1}{2}},$$
$$(r_2)_j = m_{j-1} - m_j + h_j n_{j-\frac{1}{2}},$$
$$(r_3)_j = \theta_{j-1} - \theta_j + h_j q_{j-\frac{1}{2}}\ (PST),$$
$$(r_3)_j = \Theta_{j-1} - \Theta_j + h_j q_{j-\frac{1}{2}}\ (PHF),$$
$$(r_4)_j = \phi_{j-1} - \phi_j + h_j s_{j-\frac{1}{2}},$$
$$(r_5)_j = n_{j-1} - n_j - \frac{We}{2}(n_j^2 - n_{j-1}^2) - h_j f_{j-\frac{1}{2}} n_{j-\frac{1}{2}} + h_j m_{j-\frac{1}{2}}^2 + \beta h_j\left(\frac{\eta}{2}n_{j-\frac{1}{2}} + m_{j-\frac{1}{2}}\right) + (M+\lambda)h_j m_{j-\frac{1}{2}} - Fr h_j m_{j-\frac{1}{2}}^2 - h_j G(\theta_{j-\frac{1}{2}} + N\phi_{j-\frac{1}{2}}),$$
$$(r_6)_j = q_{j-1} - q_j - h_j\frac{N_c}{Le}s_{j-\frac{1}{2}}q_{j-\frac{1}{2}} - h_j\frac{N_c}{LeN_{bt}}q_{j-\frac{1}{2}}^2 + h_j Pr(\beta\left(\frac{\eta}{2}q_{j-\frac{1}{2}} + \theta_{j-\frac{1}{2}}\right) + u_{j-\frac{1}{2}}\theta_{j-\frac{1}{2}} - f_{j-\frac{1}{2}}q_{j-\frac{1}{2}})\ (PST),$$

$$(r_6)_j = q_{j-1} - q_j - h_j\frac{N_c}{Le}s_{j-\frac{1}{2}}q_{j-\frac{1}{2}} - h_j\frac{N_c}{LeN_{bt}}q_{j-\frac{1}{2}}^2 + h_j Pr(\frac{\beta}{2}(\eta q_{j-\frac{1}{2}} + \Theta_{j-\frac{1}{2}}) + m_{j-\frac{1}{2}}\Theta_{j-\frac{1}{2}} - f_{j-\frac{1}{2}}q_{j-\frac{1}{2}})\ (PHF),$$

$$(r_7)_j = s_{j-1} - s_j + h_j Sc\left(\beta\left(\frac{\eta}{2}s_{j-\frac{1}{2}} + \phi_{j-\frac{1}{2}}\right) + m_{j-\frac{1}{2}}\phi_{j-\frac{1}{2}} - f_{j-\frac{1}{2}}s_{j-\frac{1}{2}}\right) - \frac{1}{N_{bt}}(q_j - q_{j-1}).$$

For iterates, the boundary conditions (34 - 35) take the following form respectively:

$$\left.\begin{array}{llll} \delta f_0 = 0, & \delta m_0 = 0, & \delta\theta_0 = 0, & \delta\phi_0 = 0, \\ \delta m_J = 0, & \delta\theta_J = 0, & \delta\phi_J = 0. & \end{array}\right\} \tag{38}$$

$$\left.\begin{array}{llll} \delta f_0 = 0, & \delta m_0 = 0, & \delta q_0 = 0, & \delta\phi_0 = 0, \\ \delta m_J = 0, & \delta\Theta_J = 0, & \delta\phi_J = 0. & \end{array}\right\} \tag{39}$$

Block tridiagonal structure

The linearized system of equations (37) can be written in the matrix form as:

$$\begin{bmatrix} [A_1] & [C_1] & & & & & & \\ [B_2] & [A_2] & [C_2] & & & & & \\ & [B_3] & [A_3] & [C_3] & & & & \\ & & & \ddots & \cdots & & & \\ & & & & [B_{j-1}] & [A_{j-1}] & [C_{j-1}] & \\ & & & & & [B_j] & [A_j] \end{bmatrix} \begin{bmatrix} [\delta_1] \\ [\delta_2] \\ [\delta_3] \\ \vdots \\ [\delta_{j-1}] \\ [\delta_J] \end{bmatrix} = \begin{bmatrix} [r_1] \\ [r_2] \\ [r_3] \\ \vdots \\ [r_{j-1}] \\ [r_j] \end{bmatrix}$$

or

$$[A][\delta] = [r] \tag{40}$$

where the elements for both prescribed heat mechanisms are respectively:

$$[\delta_1] = \begin{bmatrix} [\delta n_0] \\ [\delta q_0] \\ [\delta s_0] \\ [\delta f_1] \\ [\delta n_1] \\ [\delta q_1] \\ [\delta s_1] \end{bmatrix}, \quad [\delta_j] = \begin{bmatrix} [\delta m_{j-1}] \\ [\delta\theta_{j-1}] \\ [\delta\phi_{j-1}] \\ [\delta f_j] \\ [\delta n_j] \\ [\delta q_j] \\ [\delta s_j] \end{bmatrix}, \quad 2 \le j \le J, \quad [\delta_1] = \begin{bmatrix} [\delta n_0] \\ [\delta q_0] \\ [\delta s_0] \\ [\delta f_1] \\ [\delta n_1] \\ [\delta q_1] \\ [\delta s_1] \end{bmatrix},$$

$$[\delta_j] = \begin{bmatrix} [\delta u_{j-1}] \\ [\delta\Theta_{j-1}] \\ [\delta\phi_{j-1}] \\ [\delta f_j] \\ [\delta n_j] \\ [\delta q_j] \\ [\delta s_j] \end{bmatrix}, 2 \le j \le J, \qquad [r_j] = \begin{bmatrix} (r_1)_j \\ (r_2)_j \\ (r_3)_j \\ (r_4)_j \\ (r_5)_j \\ (r_6)j \\ (r_7)_j \end{bmatrix}, 1 \le j \le J$$

For PST condition:

$$[A_1] = \begin{bmatrix} 0 & 0 & 0 & 1 & 0 & 0 & 0 \\ d & 0 & 0 & 0 & d & 0 & 0 \\ 0 & d & 0 & 0 & 0 & d & 0 \\ 0 & 0 & d & 0 & 0 & 0 & d \\ (a_2)_1 & 0 & 0 & (a_3)_1 & (a_1)_1 & 0 & 0 \\ 0 & (b_2)_1 & (b_{10})_1 & (b_3)_1 & 0 & (b_1)_1 & (b_9)_1 \\ 0 & (c_{10})_1 & (c_2)_1 & (c_3)_1 & 0 & (c_9)_1 & (c_1)_1 \end{bmatrix}$$

For PHF case:

$$[A_1] = \begin{bmatrix} 0 & 0 & 0 & 1 & 0 & 0 & 0 \\ d & 0 & 0 & 0 & d & 0 & 0 \\ 0 & -1 & 0 & 0 & 0 & d & 0 \\ 0 & 0 & d & 0 & 0 & 0 & d \\ (a_2)_1 & (a_8)_1 & 0 & (a_3)_1 & (a_1)_1 & 0 & 0 \\ 0 & (b_8)_1 & (b_{10})_1 & (b_3)_1 & 0 & (b_1)_1 & (b_9)_1 \\ 0 & 0 & (c_2)_1 & (c_3)_1 & 0 & (c_9)_1 & (c_1)_1 \end{bmatrix}$$

For both prescribed heat cases:

$$[A_j] = \begin{bmatrix} d & 0 & 0 & 1 & 0 & 0 & 0 \\ -1 & 0 & 0 & 0 & d & 0 & 0 \\ 0 & -1 & 0 & 0 & 0 & d & 0 \\ 0 & 0 & -1 & 0 & 0 & 0 & d \\ (a_6)_j & (a_8)_j & (a_{10})_j & (a_3)_j & (a_1)_j & 0 & 0 \\ (b_6)_j & (b_8)_j & 0 & (b_3)_j & 0 & (b_1)_j & (b_9)_j \\ (c_6)_j & 0 & (c_8)_j & (c_3)_j & 0 & (c_9)_j & (c_1)_j \end{bmatrix}, \quad 2 \le j \le J$$

$$[B_j] = \begin{bmatrix} 0 & 0 & 0 & -1 & 0 & 0 & 0 \\ 0 & 0 & 0 & 0 & d & 0 & 0 \\ 0 & 0 & 0 & 0 & 0 & d & 0 \\ 0 & 0 & 0 & 0 & 0 & 0 & d \\ 0 & 0 & 0 & (a_4)_j & (a_2)_j & 0 & 0 \\ 0 & 0 & 0 & (b_4)_j & 0 & (b_2)_j & (b_{10})_j \\ 0 & 0 & 0 & (c_4)_j & 0 & (c_{10})_j & (c_2)_j \end{bmatrix}, \quad 2 \le j \le J$$

$$[C_j] = \begin{bmatrix} d & 0 & 0 & 0 & 0 & 0 & 0 \\ 1 & 0 & 0 & 0 & 0 & 0 & 0 \\ 0 & 1 & 0 & 0 & 0 & 0 & 0 \\ 0 & 0 & 1 & 0 & 0 & 0 & 0 \\ (a_5)_j & (a_7)_j & (a_9)_j & 0 & 0 & 0 & 0 \\ (b_5)_j & (b_7)_j & 0 & 0 & 0 & 0 & 0 \\ (c_5)_j & 0 & (c_7)_j & 0 & 0 & 0 & 0 \end{bmatrix}, \ 1 \le j < J$$

Here $d = -\frac{h_j}{2}$.

Now, we will solve equation (40) by LU decomposition, for that we assume A is non-singular matrix and can be factored into:

$$[A] = [L][U] \tag{41}$$

where

$$[L] = \begin{bmatrix} [\alpha_1] & & & & \\ [\beta_2] & [\alpha_2] & & & \\ & \ddots & \ddots & & \\ & & [\alpha_{J-1}] & & \\ & & [\beta_J] & [\alpha_J] \end{bmatrix}, \ [U] = \begin{bmatrix} [I_1] & [\Gamma_1] & & & \\ & [I] & [\Gamma_2] & & \\ & & \ddots & \ddots & \\ & & & [I] & [\Gamma_{J-1}] \\ & & & & [I] \end{bmatrix}$$

These $[\alpha_j]$, $[\Gamma_j]$ and $[\beta_j]$ are 7×7 ordered matrices from which their elements are determined by following equations:

$$\left.\begin{array}{c} [\alpha_1] = [A_1] \\ [A_1][\Gamma_1] = [C_1] \\ [\alpha_j] = [A_j] - [\beta_j][\Gamma_{j-1}], \ j = 2,3,\ldots J \\ [A_j][\Gamma_j] = [C_j], \ j = 2,3,\ldots J \end{array}\right\} \tag{42}$$

By substituting equation (41) in (40), we get

$$[L][U][\delta] = [r] \tag{43}$$

Now assuming,

$$[U][\delta] = [W] \tag{44}$$

therefore, equation (43) becomes

$$[L][W] = [r], \tag{45}$$

where

$$[W] = \begin{bmatrix} [W_1] \\ [W_2] \\ \vdots \\ [W_{j-1}] \\ [W_j] \end{bmatrix}, \ 1 \le j \le J$$

Here $[W_j]$ are column matrices of order 7×1 and elements can be obtained by solving equation (45) such as:

$$[\alpha_1][W_1] = [r_1], \ \ [\alpha_j][W_j] = [r_j] - [\beta_j][W_{j-1}], \ 2 \le j \le J. \tag{46}$$

The elements of Γ_j, α_j and W_j are calculated by applying forward sweep, after that the elements of δ is easily calculated from the equation (44) by using backward sweep and the elements are:

$$[\delta_J] = [W_J], \ \ [\delta_j] = [W_j] - [\Gamma_j][\delta_{j+1}], \ 1 \le j \le J - 1. \tag{47}$$

These iteration processes are repeated until the desired convergence criterion is obtained i.e. $|\delta {v_0}^{(i)}| < \epsilon$, where ϵ is desired level of accuracy.

6 Discussion on results and outcomes

This section presents the effects of key dimensionless parameters β, N, G, Fr, L, We, N_{bt}, N_c, Sc, Pr, Le, and ϵ—on velocity $f'(\eta)$, temperature $\theta(\eta)$, and nanoparticle concentration $\phi(\eta)$, illustrated through graphical results. For validation, a comparison (Table:1) is made with previous studies by Mahapatra and Gupta [26], Nazar et al. [34], Ishak et al. [14], and Thakur and Sood [3]. The strong agreement confirms the accuracy and reliability of the present numerical results.

ϵ	Mahapatra & Gupta[26]	Nazar et al.[34]	Ishak et al.[14]	Thakur & Sood [3]	Present study
0.10	-0.9694	-0.9694	-0.9694	-0.9694	-0.9694
0.20	-0.9181	-0.9181	-0.9181	-0.9181	-0.9181
0.50	-0.6673	-0.6673	-0.6673	-0.6673	-0.6673
2.00	2.0176	2.0176	2.0175	2.0187	2.0187

Table 1: A comparative analysis of values of $f''(0)$ for different values of ϵ where $We = Fr = \lambda = M = \beta = G = N = S_1 = S_2 = 0$

ISSN: 1001-4055

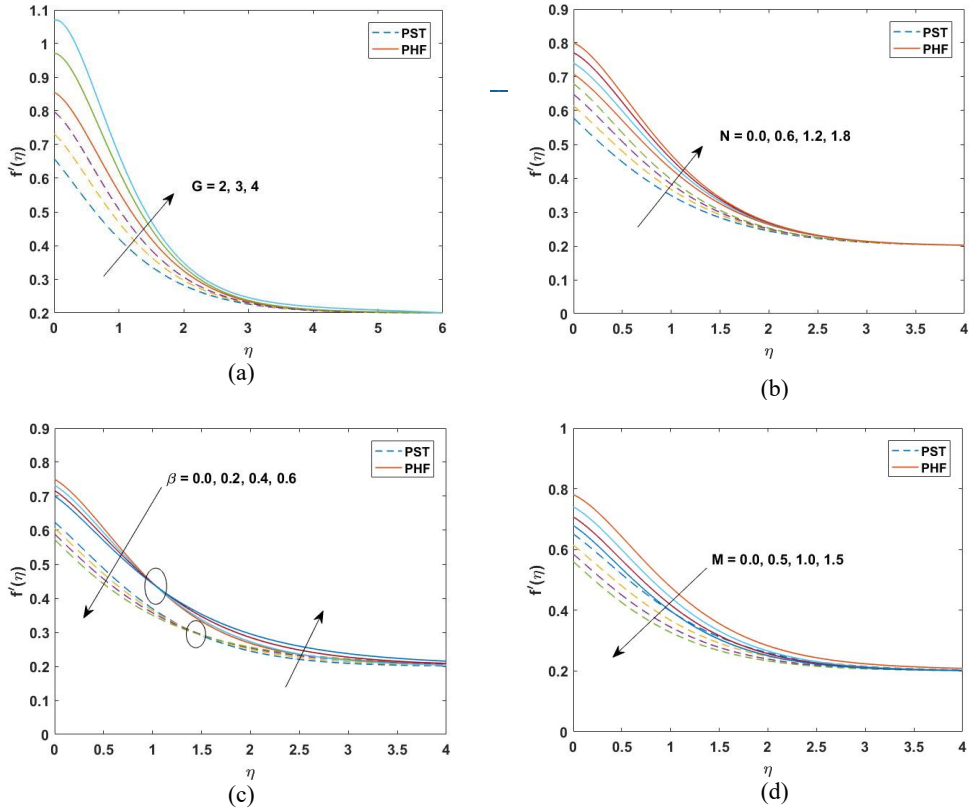

6.1 Findings

To analyze the problem's physics, the following parameter values are fixed unless stated otherwise: $M = 0.5$, $We = 0.2$, $Fr = 0.2$, $\lambda = 0.5$, $\epsilon = 0.2$, $Le = 5$, $Pr = 2$, $N_{bt} = 2$, $N_c = 2.5$, $Sc = 5$, $\beta = 0.1$, $N = 0.6$, $G = 2$, $S_1 = 0.5$, $S_2 = 0.5$. Graphs provide a comparative view of the two heat transfer cases: PST and PHF. The effects of G, N, β, and M on velocity $f'(\eta)$ are shown in Figure 1. Figure 1a indicates that increasing G enhances $f'(\eta)$ due to stronger viscous forces and greater temperature gradients near the wall, which intensify fluid motion. Similarly, Figure 1b shows that rising N boosts velocity, as buoyancy forces increase with decreasing fluid temperature. In Figure 1c, unsteadiness ($\beta > 0$) initially reduces $f'(\eta)$ near the surface, thinning the momentum boundary layer, but farther from the surface, velocity increases due to temporal effects. Finally, Figure 1d demonstrates that higher M reduces velocity, as the Lorentz force resists fluid motion.

Figure 1: The velocity profiles $f'(\eta)$ for deviating values of G, N, β and M.

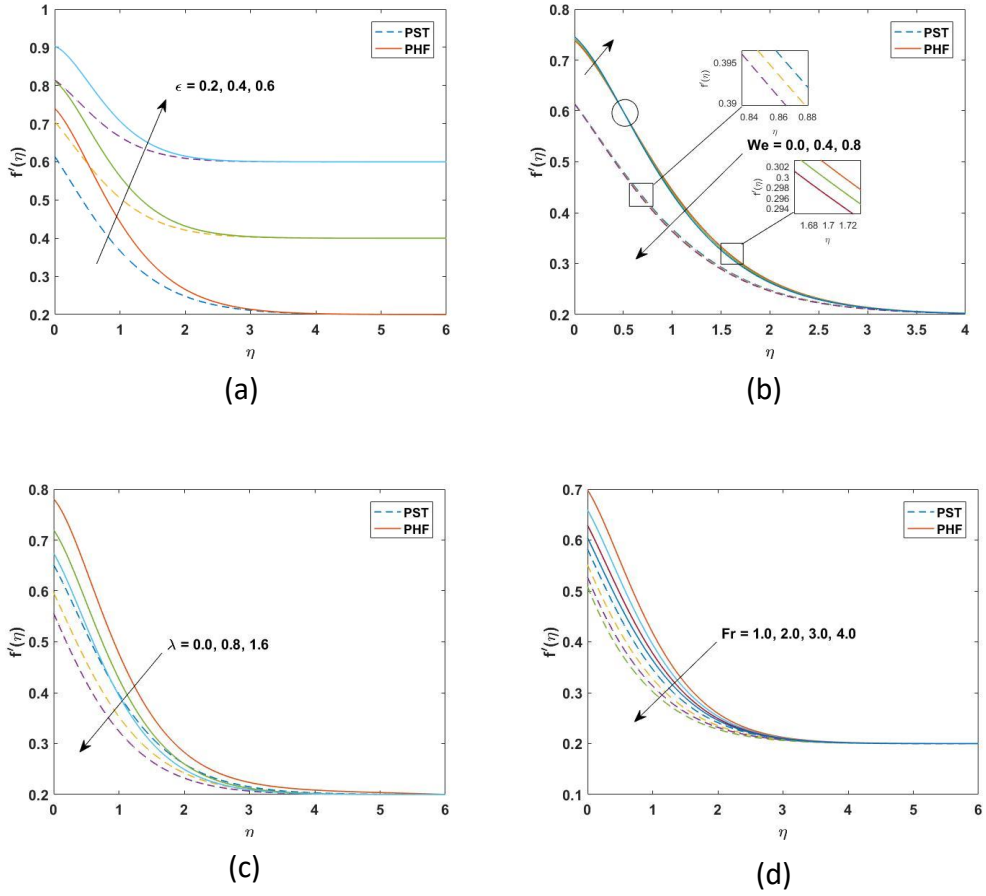

Figure 2: The velocity profiles $f'(\eta)$ for deviating values of ϵ, We, λ and Fr.

Figure 2 illustrates the effects of ϵ, We, λ, and Fr on the velocity profile $f'(\eta)$. As shown in Figure 2a, increasing ϵ $(0 < \epsilon < 1)$ enhances fluid motion near the surface and thickens the velocity boundary layer. In Figure 2b, $f'(\eta)$ decreases with rising We, since a higher Williamson parameter reduces the fluid's relaxation time, leading to slower motion. Figure 2c shows a decline in velocity with increasing λ, attributed to increased flow resistance due to higher porosity, which also thins the momentum boundary layer. Lastly, Figure 2d reveals that greater Forchheimer numbers reduce $f'(\eta)$ due to lower permeability, which restricts fluid movement through the porous medium. Figure 3a shows that increasing ϵ leads to a sharp decline in the temperature profile $\theta(\eta)$ due to enhanced fluid velocity, which promotes faster

heat diffusion and reduces fluid temperature. In contrast, Figure 3b illustrates that higher porosity restricts flow, raising $\theta(\eta)$ and thickening the thermal boundary layer. As seen in Figure 3c, $\theta(\eta)$ increases with the Forchheimer number Fr, as greater drag (linked to higher C_b) elevates thermal resistance. Finally, Figure 3d reveals that rising magnetic parameter M boosts $\theta(\eta)$, attributed to the Lorentz force, which suppresses fluid motion and increases surface temperature.

Figure 4a shows that increasing the thermal convection parameter G reduces $\theta(\eta)$ and thins the thermal boundary layer due to stronger temperature gradients. Similarly, Figure 4b reveals a decline in $\theta(\eta)$ with higher buoyancy ratio N, as enhanced buoyancy-driven flow intensifies convective heat transfer. In Figure 4c, $\theta(\eta)$ initially decreases near the surface with rising unsteadiness parameter β, due to suppressed heat diffusion. However, beyond a certain distance, the profile reverses, showing an increase in temperature as the thermal effects dominate further from the surface. Figure 5a shows that increasing ε leads to a sharp decline in the temperature profile θ(η) due to enhanced fluid velocity, which promotes faster heat diffusion and reduces fluid temperature. In contrast, Figure 5b illustrates that higher porosity restricts flow, raising θ(η) and thickening the thermal boundary layer. As seen in Figure 5c, θ(η) increases with the Forchheimer number Fr, as greater drag (linked to higher C_b) elevates thermal resistance. Finally, Figure 5d reveals that rising magnetic parameter M boosts θ(η), attributed to the Lorentz force, which suppresses fluid motion and increases surface temperature.

Figure 6a shows that increasing ϵ reduces the nanoparticle concentration $\phi(\eta)$ due to enhanced external flow, which diminishes the fluid volume fraction. In Figure 6b, higher local porosity parameter λ leads to increased $\phi(\eta)$, likely due to pressure-driven outward movement of nanoparticles near the wall. Figure 6c indicates that $\phi(\eta)$ rises with Forchheimer number Fr, and Figure 6d reveals a similar trend with the magnetic parameter M. A stronger magnetic field slows fluid motion, promoting nanoparticle accumulation within the porous medium.

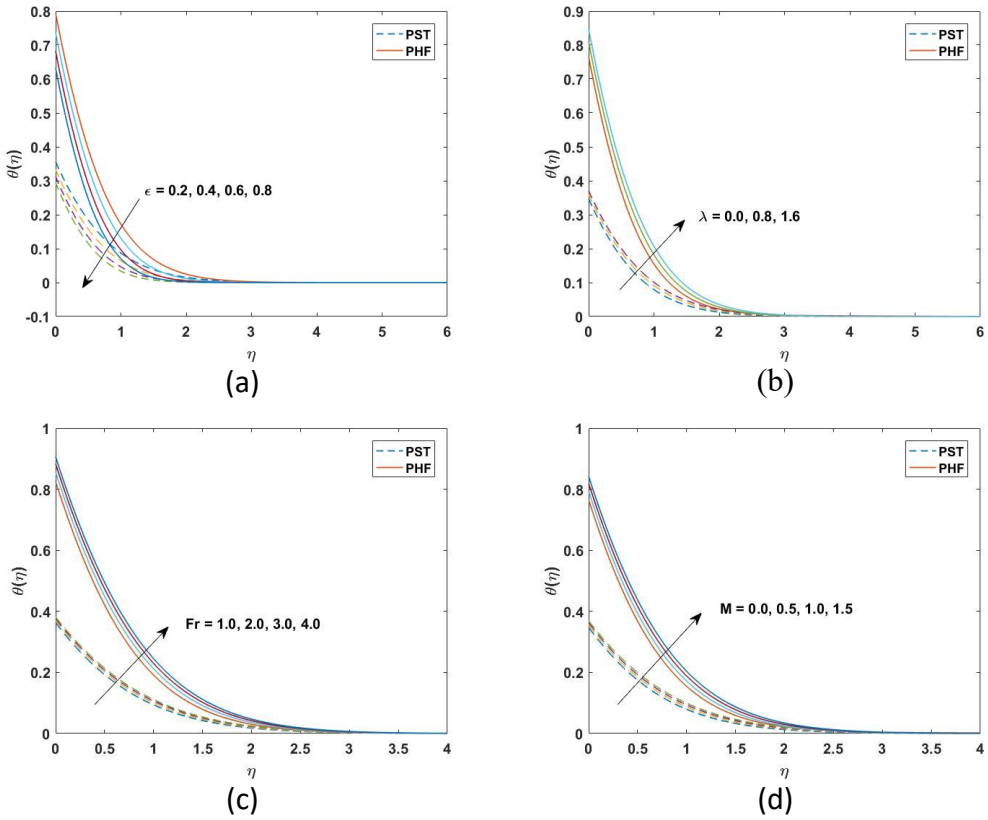

Figure 3: The temperature profiles $\theta(\eta)$ for deviating values of ϵ, λ, Fr, and M.

Figure 7a shows that increasing the thermophoresis parameter N_{bt} leads to a decline in $\phi(\eta)$, as intensified particle motion causes greater dispersion and collisions. As seen in Figure 7b, higher Schmidt number Sc —which inversely relates to Brownian diffusivity—reduces nanoparticle concentration due to limited diffusion. Figure 7c illustrates that rising unsteadiness parameter β lowers $\phi(\eta)$, likely due to reduced heat and mass transfer from the stretching surface. Figures Figure 7d and Figure 7e also show decreasing concentration with increasing G and N, as stronger convection and buoyancy enhance dispersion, reducing accumulation near the surface.

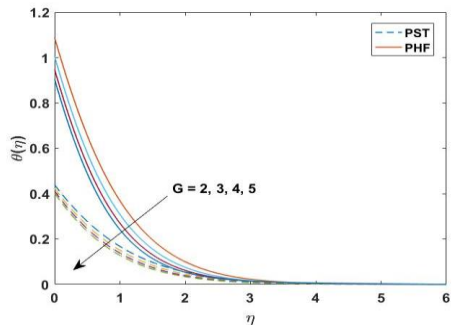

(a)

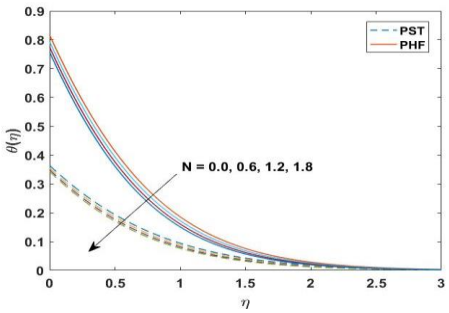

(b)

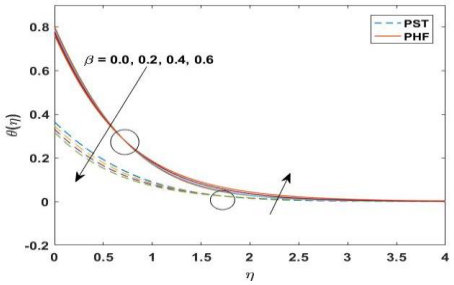

(c)

Figure 4: The temperature profiles $\theta(\eta)$ for deviating values of G, N and β.

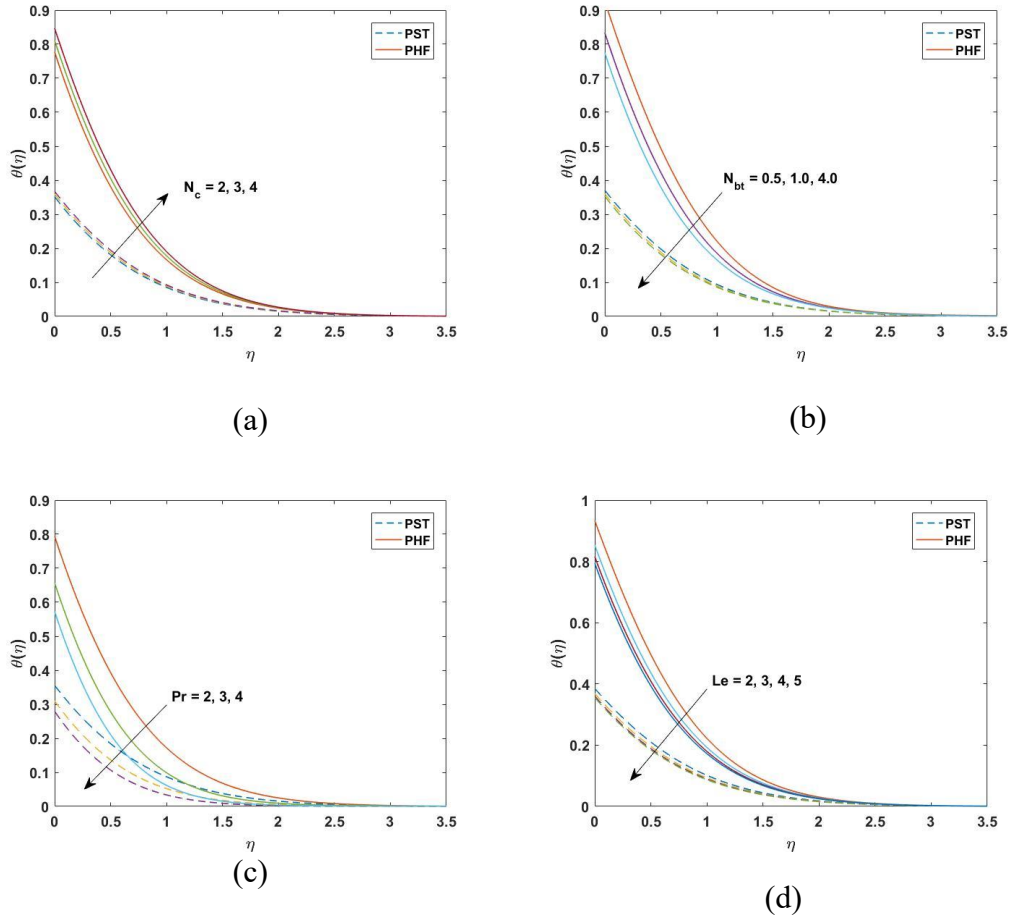

Figure 5: The temperature profiles $\theta(\eta)$ for deviating values of N_c, N_{bt}, Pr, and Le.

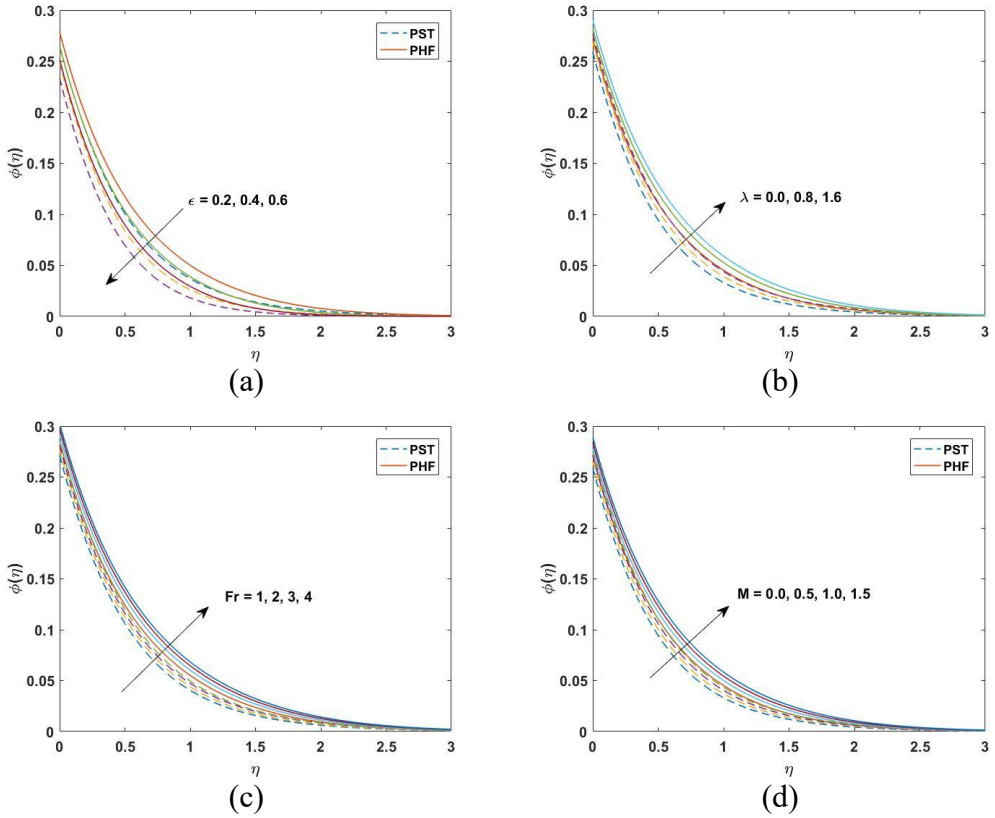

Figure 6: The concentration profiles $\phi(\eta)$ for deviating values of ϵ, λ, Fr and M.

Figure 8 illustrates how the skin-friction coefficient $C_{fx}(Re)^{1/2}$ varies with We and ϵ under different values of λ, Fr, G, and β. As shown in Figure 8a and Figure 8b, $C_{fx}(Re)^{1/2}$ increases with higher We and Fr, but decreases as λ increases, with consistent trends observed for both PST and PHF cases. In Figure 8c and Figure 8d, $C_{fx}(Re)^{1/2}$ rises with increasing ϵ and G, while a slight decline is noted for increasing β. The influence of G is more pronounced compared to that of β.

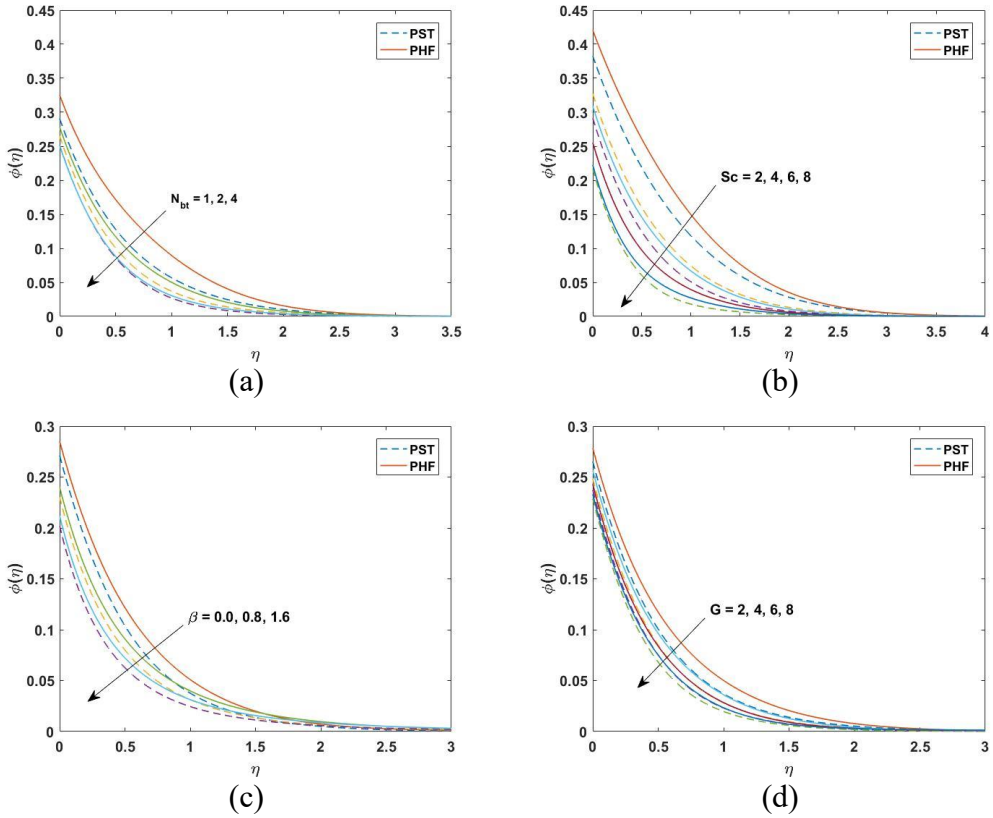

Figure 7: The concentration profiles $\phi(\eta)$ for deviating values of N_{bt}, Sc, β, and G.

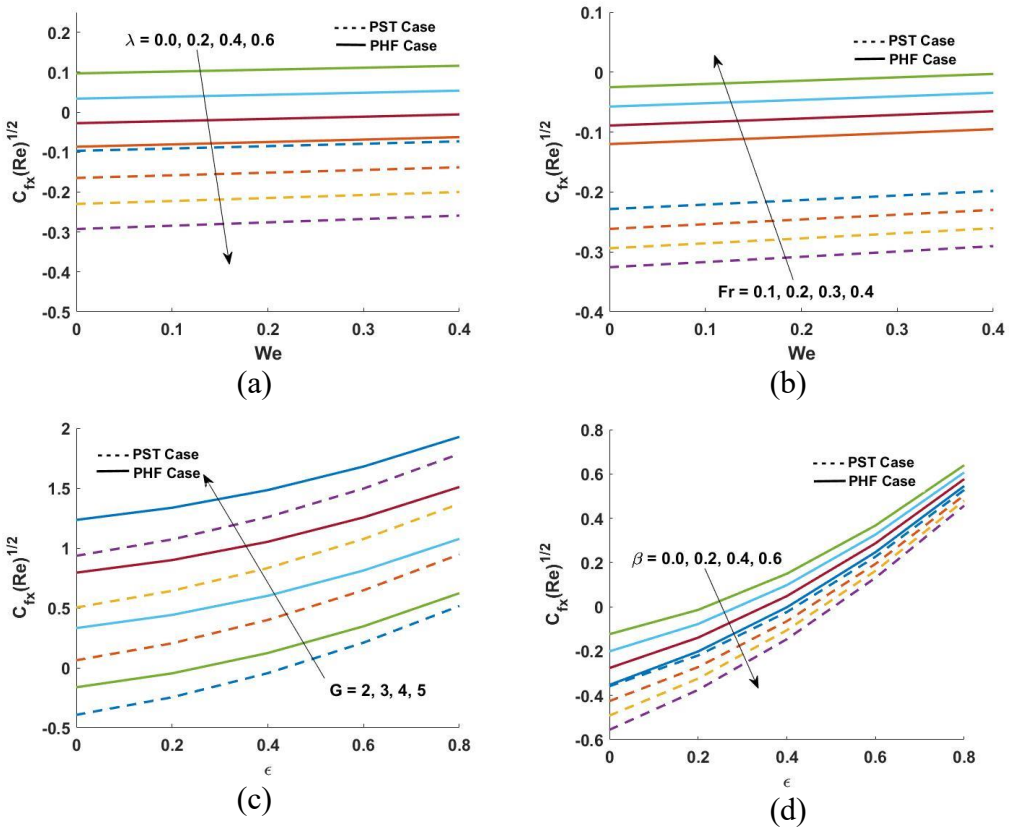

Figure 8: The variation of $C_{fx}Re^{\frac{1}{2}}$ with We and ϵ for deviating values of λ, Fr, G and β.

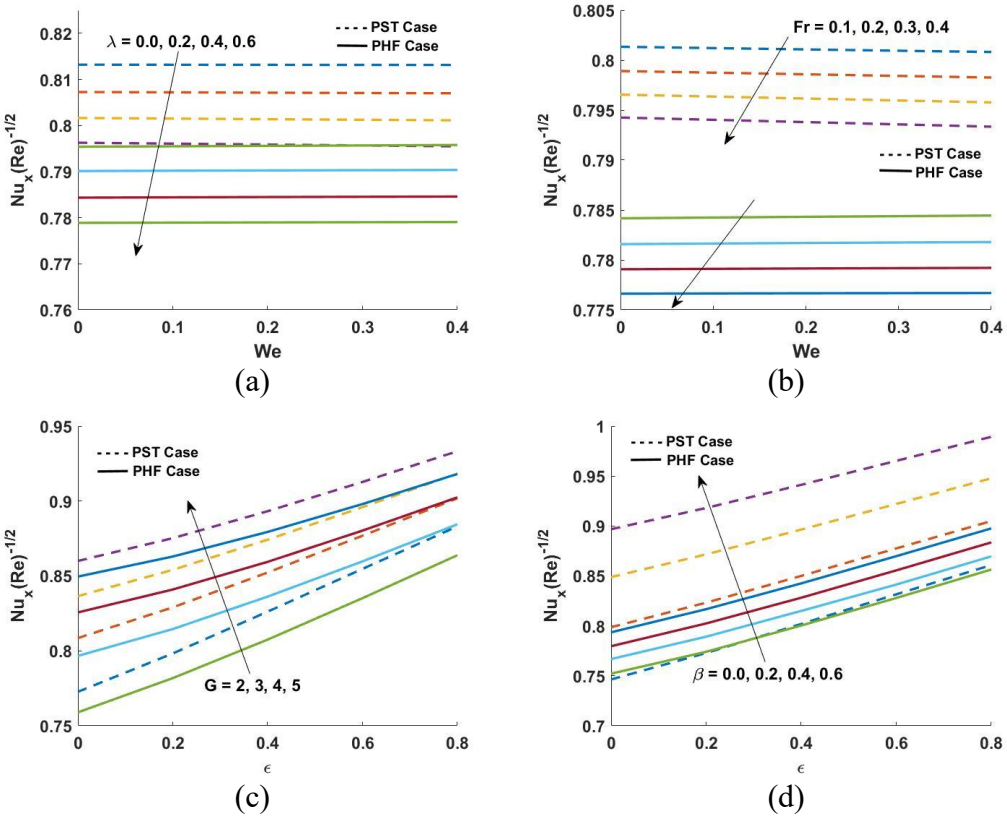

Figure 9: The variation of $Nu_x Re^{-\frac{1}{2}}$ with We and ϵ for deviating values of λ, Fr, G and β.

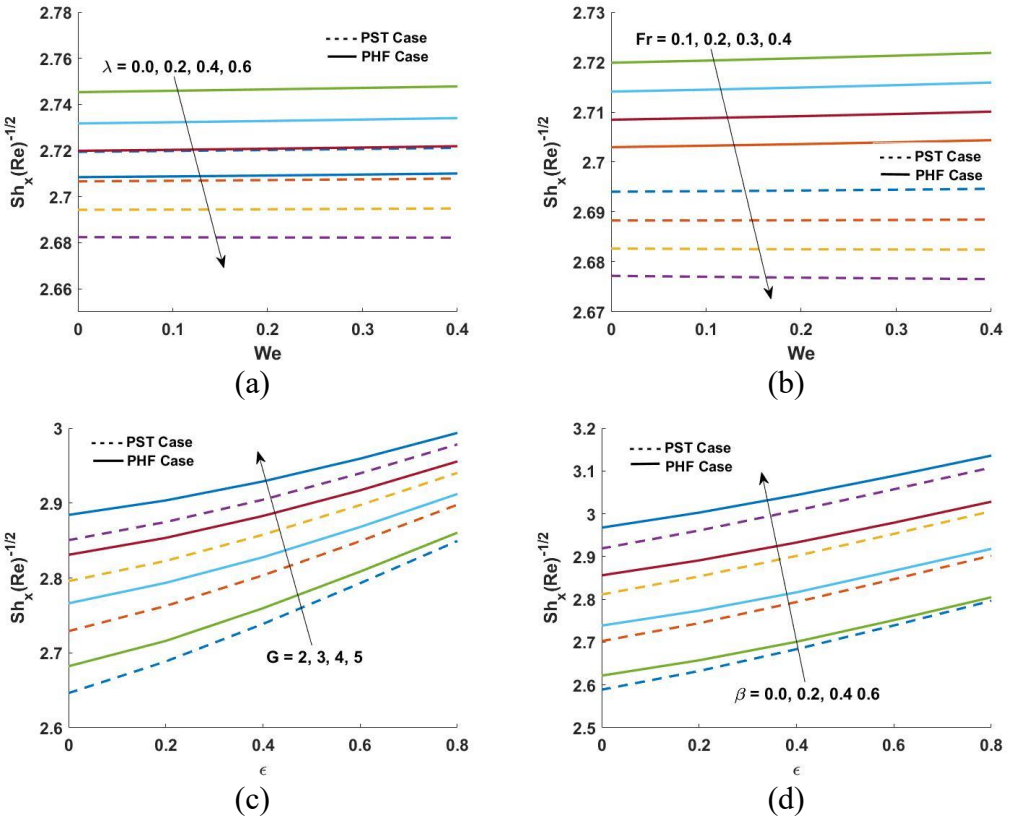

Figure 10: The variation of $Sh_x Re^{-\frac{1}{2}}$ with We and ϵ for deviating values of λ, Fr, G and β.

Figure 9 shows the variation of the local Nusselt number $Nu_x(Re)^{-1/2}$ with respect to We and ϵ for different values of λ, Fr, G, and β. Figures 9a and 9b reveal a uniform decline in $Nu_x(Re)^{-1/2}$ with increasing We, Fr, and λ. Conversely, 9c and 9d show that $Nu_x(Re)^{-1/2}$ increases with higher ϵ, G, and β. These trends are linked to enhanced temperature gradients between the sheet and the fluid, and increased external flow, which accelerates heat transfer near the surface. While the effect of β is moderate under PHF conditions, it is more prominent in PST. Overall, heat transfer improves in both PST and PHF cases with increasing G and β. Figure 10 illustrates how the local Sherwood number $Sh_x(Re)^{-1/2}$ varies with We and ϵ under different values of λ, Fr, G, and β. Figures 10a and 10b show a slight but consistent decrease in $Sh_x(Re)^{-1/2}$ with increasing We, Fr, and λ for both PST and PHF cases. In contrast, Figures 10c and 10d demonstrate that $Sh_x(Re)^{-1/2}$ rises with higher values of ϵ, G, and β.

7 Concluding Remarks

This study presents a computational model for the stagnation point flow of Williamson nanofluid over a linearly stretching sheet embedded in a porous medium, using the Darcy–Forchheimer framework. The main objective is to analyze the influence of key physical

parameters on flow, heat, and mass transfer under both PST and PHF conditions. The graphical results provide clear insights, with each figure comparing both thermal cases. The key conclusions are as follows:

• In both PST and PHF heat transfer cases, the porous medium reduces momentum boundary layer thickness while increasing thermal thickness. Velocity and temperature profiles exhibit similar trends with unsteadiness but differ for other parameters, whereas concentration profiles remain largely consistent across all parameters such as G, N, λ, ϵ, β, and M.

• An increase in unsteadiness, thermal convection parameter, and velocity ratio enhances the local Nusselt number, indicating improved heat transfer—more significantly in the PST case than in PHF. Enhanced heat transfer under such conditions is useful in thermal management systems, such as cooling of electronics or heat exchangers using nanofluids.

• In both PST and PHF scenarios, higher permeability favors conductive heat transfer, as fluid resistance decreases. This behavior is applicable in porous heat sinks and energy systems where efficient conduction through porous materials is essential.

• The local Sherwood number increases with rising unsteadiness, thermal convection, and velocity ratio parameters, indicating enhanced convective mass transfer. This effect is particularly beneficial in applications such as membrane filtration, chemical reactors, and drug delivery systems, where efficient solute transport is critical.

References

[1] Aamir, H., Khan, M., Heat and mass transport phenomena of nanoparticles on time-dependent flow of Williamson fluid towards heated surface, *Neural Comput. Appl.* **32**(8) (2020) 3253–3263. DOI: https://doi.org/10.1007/s00521-019-04100-4

[2] Akbar, N. S., Hayat, T., Nadeem, S., Obaidat, S., Peristaltic flow of a Williamson fluid in an inclined asymmetric channel with partial slip and heat transfer, *Int. J. Heat Mass Transf.* **55**(7–8) (2012) 1855–1862. DOI: https://doi.org/10.1016/j.ijheatmasstransfer.2011.11.038

[3] Thakur, A., Sood, S., Effect of Prescribed Heat Sources on Convective Unsteady MHD Flow of Williamson Nanofluid Through Porous Media: Darcy–Forchheimer Model, *Int. J. Appl. Comput. Math.* **8**(2) (2022) 1–24. DOI: https://doi.org/10.1007/s40819-022-01271-y

[4] Attia, H. A., On the effectiveness of porosity on stagnation point flow with heat transfer over a permeable surface, *J. Por. Media* **10**(6) (2007) 625–631. DOI: 10.1615/JPorMedia.v10.i6.80

[5] Singh, B., Sood, S., Thakur, A., Chandel, S., Numerical analysis of mixed convection and Thomson–Troian slip effects on ternary nanofluid flow and heat transfer over a stretching sheet with porous media: Darcy–Forchheimer model, *Appl. Comput. Mech.* **18**(2) (2024). DOI: https://doi.org/10.24132/acm.2024.894

[6] Eldabe, N. T., Elogail, M. A., Elshaboury, S. M., Hasan, A. A., Hall effects on the peristaltic transport of Williamson fluid through a porous medium with heat and mass transfer, *Appl. Math. Model.* **40**(1) (2016) 315–328. DOI: https://doi.org/10.1016/j.apm.2015.04.043

[7] Ellahi, R., Riaz, A., Nadeem, S., Three dimensional peristaltic flow of Williamson fluid in a rectangular duct, *Indian J. Phys.* **87**(12) (2013) 1275–1281. DOI: https://doi.org/10.1007/s12648-013-0340-2

[8] Ganesh, N. V., Hakeem, A. A., Ganga, B., Darcy–Forchheimer flow of hydromagnetic nanofluid over a stretching/shrinking sheet in a thermally stratified porous medium with second order slip, viscous and Ohmic dissipations effects, *Ain Shams Eng. J.* **9**(4) (2018) 939–951. DOI: https://doi.org/10.1016/j.asej.2016.04.019

[9] Van Gorder, R. A., Sweet, E., Vajravelu, K., Nano boundary layers over stretching surfaces, *Commun. Nonlinear Sci. Numer. Simul.* **15**(6) (2010) 1494–1500. https://doi.org/10.1016/j.cnsns.2009.06.004

[10] Goyal, M., Bhargava, R., Boundary layer flow and heat transfer of viscoelastic nanofluids past a stretching sheet with partial slip conditions, *Appl. Nanosci.* **4**(6) (2013) 761–767. DOI: https://doi.org/10.1007/s13204-013-0254-5

[11] Hamid, A., Khan, M., Hafeez, A., Unsteady stagnation-point flow of Williamson fluid generated by stretching/shrinking sheet with Ohmic heating, *Int. J. Heat Mass Transf.* **126** (2018) 933–940. DOI: https://doi.org/10.1016/j.ijheatmasstransfer.2018.05.076

[12] Hamid, M., Usman, M., Khan, Z. H., Haq, R. U., Wang, W., Numerical study of unsteady MHD flow of Williamson nanofluid in a permeable channel with heat source/sink and thermal radiation, *Eur. Phys. J. Plus* **133**(12) (2018) 1–12. DOI: https://doi.org/10.1140/epjp/i2018-12322-5

[13] Hashim, H., Mohamed, M. K. A., Ishak, N., Sarif, N. M., Salleh, M. Z., Thermal radiation effect on MHD stagnation point flow of Williamson fluid over a stretching surface, *J. Phys.* **1366**(1) (2019) 207–217. DOI: 10.1088/1742-6596/1366/1/012011

[14] Ishak, A., Nazar, R., Arifin, N. M., Pop, I., Mixed convection of the stagnation-point flow towards a stretching vertical permeable sheet, *Malaysian J. Math. Sci.* **2** (2007) 217–226. Available at: https://mjms.upm.edu.my/lihatmakalah.php?kod=2007/July/1/2/217-226

[15] Jamshed, W., Eid, M. R., Shahzad, F., Safdar, R., Shamshuddin, M. D., Keller box analysis for thermal efficiency of magneto time-dependent nanofluid flowing in solar-powered tractor application applying nano-metal shaped factor, *Waves Random Complex Media* (2022) 1–36. DOI: https://doi.org/10.1080/17455030.2022.2146779

[16] Kebede, T., Haile, E., Awgichew, G., Walelign, T., Heat and mass transfer in unsteady boundary layer flow of Williamson nanofluids, *J. Appl. Math.* (2020). DOI: https://doi.org/10.1155/2020/1890972

[17] Kiyani, M. Z., Aeman, A., Abbasi, A., Ullah Khan, S., Eladeb, A., Kolsi, L., Mebarek-Oudina, F., Analysis of Nanofluid Through Porous Media with Darcy–Forchheimer and Mass Suction Effects: Keller Box Numerical Simulations, *J. Nanofluids* **14**(3) (2025) 438–446. DOI: https://doi.org/10.1166/jon.2025.2252

[18] Khader, M. M., Ahmad, H., Adel, M., Megahed, A. M., Numerical analysis of the MHD Williamson nanofluid flow over a nonlinear stretching sheet through a Darcy porous medium: Modeling and simulation, *Open Phys.* **22**(1) (2024) 20240016. DOI: https://doi.org/10.1515/phys-2024-0016

[19] Kho, Y. B., Hussanan, A., Mohamed, M. K. A., Salleh, M. Z., Heat and mass transfer analysis on flow of Williamson nanofluid with thermal and velocity slips: Buongiorno model, *Propul. Power Res.* **8**(3) (2019) 243–252. DOI: https://doi.org/10.1016/j.jppr.2019.01.011

[20] Khan, N. A., Khan, H., A boundary layer flows of non-Newtonian Williamson fluid, *Nonlinear Eng.* **3**(2) (2014) 107–115. Available on: https://www.degruyterbrill.com/document/doi/10.1515/nleng-2014-0002/html

[21] Khan, N. A., Khan, S., Riaz, F., Boundary layer flow of Williamson fluid with chemically reactive species using scaling transformation and homotopy analysis method, *Math. Sci. Lett.* **3**(3) (2014) 199. DOI: http:dx.doi.org/10.12785/msl/030311

[22] Kumar, R., Kumar, R., Vajravelu, K., Sheikholeslami, M., Three dimensional stagnation flow of Casson nanofluid through Darcy–Forchheimer space: A reduction to Blasius/Sakiadis flow, *Chin. J. Phys.* **68** (2020) 874–885. DOI: https://doi.org/10.1016/j.cjph.2020.10.027

[23] Laxmaiah, K., Reddy, Y. D., Thermal radiation and chemical reaction effects on MHD Williamson nanofluid flow over an exponentially porous stretching sheet with non-uniform heat source/sink, *J. Radiat. Res. Appl. Sci.* **18**(3) (2025) 101742. DOI: https://doi.org/10.1016/j.jrras.2025.101742

[24] Ramamoorthy, M., Pallavarapu, L., Radiation and Hall effects on a 3D flow of MHD Williamson fluid over a stretchable surface, *Heat Transf.* **49**(8) (2020) 4410–4426. DOI:

https://doi.org/10.1002/htj.21833

[25] Meenakumari, R., Lakshminarayana, P., Vajravelu, K., Unsteady MHD flow of a Williamson nanofluid on a permeable stretching surface with radiation and chemical reaction effects, *Eur. Phys. J. Spec. Top.* **230** (2021) 1355–1370. DOI: https://doi.org/10.1140/epjs/s11734-021-00039-7

[26] Mahapatra, T. R., Gupta, A. S., Heat transfer in the stagnation-point flow towards a stretching sheet, *Heat Mass Transf.* **38**(6) (2002) 517–521. DOI: https://doi.org/10.1007/s002310100215

[27] Majeed, A., Zeeshan, A., Noori, F. M., Numerical study of Darcy–Forchheimer model with activation energy subject to chemically reactive species and momentum slip of order two, *AIP Adv.* **9**(4) (2019) 045035. DOI: https://doi.org/10.1063/1.5095546

[28] Malvandi, A., Hedayati, F., Ganji, D. D., Slip effects on unsteady stagnation point flow of a nanofluid over a stretching sheet, *Powder Technol.* **253** (2014) 377–384. DOI: https://doi.org/10.1016/j.powtec.2013.11.049

[29] Mishra, S. R., Shamshuddin, M. D., Panda, S., Ibrahim, W., Baithalu, R., Keller Box investigation of hybrid nanofluid flow using aluminum alloys over radiative Riga plate surface subjected to variable porous medium, *Sci. Iran.* (2025). DOI: 10.24200/sci.2025.65527.9536

[30] Mohammed, A. A., Dawood, A. S., Mixed convection heat transfer in a ventilated enclosure with and without a saturated porous medium, *J. Por. Media* **19**(4) (2016) 347–366. DOI: 10.1615/JPorMedia.v19.i4.60

[31] Mukhopadhyay, S., Slip effects on MHD boundary layer flow over an exponentially stretching sheet with suction/blowing and thermal radiation, *Ain Shams Eng. J.* **4**(3) (2013) 485–491. DOI: https://doi.org/10.1016/j.asej.2012.10.007

[32] Nadeem, S., Akram, S., Peristaltic flow of a Williamson fluid in an asymmetric channel, *Commun. Nonlinear Sci. Numer. Simul.* **15**(7) (2010) 1705–1716. DOI: https://doi.org/10.1016/j.cnsns.2009.07.026

[33] Nadeem, S., Hussain, S. T., Flow and heat transfer analysis of Williamson nanofluid, *Appl. Nanosci.* **4**(8) (2014) 1005–1012. DOI: https://doi.org/10.1016/j.cnsns.2009.07.026

[34] Nazar, R., Amin, N., Filip, D., Pop, I., Stagnation point flow of a micropolar fluid towards a stretching sheet, *Int. J. Non-Linear Mech.* **39**(7) (2004) 1227–1235. DOI: https://doi.org/10.1016/j.ijnonlinmec.2003.08.007

[35] Noghrehabadi, A., Pourrajab, R., Ghalambaz, M., Effect of partial slip boundary condition on the flow and heat transfer of nanofluids past stretching sheet prescribed constant wall temperature, *Int. J. Therm. Sci.* **54** (2012) 253–261. DOI: https://doi.org/10.1016/j.ijthermalsci.2011.11.017

[36] Olkha, A., Kumar, M., Meena, S. K., Effects of Heat Transport Characteristics and Chemical Reaction in Unsteady Flow of Williamson Fluid and Entropy Generation: The Keller-Box Numerical Scheme, *Heat Transf.* **54**(3) (2025) 2218–2234. DOI: https://doi.org/10.1002/htj.23287

[37] Pal, D., Mondal, H., Hydromagnetic convective diffusion of species in Darcy–Forchheimer porous medium with non-uniform heat source/sink and variable viscosity, *Int. Commun. Heat Mass Transf.* **39**(7) (2012) 913–917. DOI: https://doi.org/10.1016/j.icheatmasstransfer.2012.05.012

[38] Prasad, S., Sood, S., Thakur, A., Stagnation-Point Slip Flow of Hybrid Ferrofluid Past Exponentially Stretching Sheet in Darcy–Forchheimer Space, *Indian J. Sci. Technol.* **17**(10) (2024) 881–890. DOI: https://doi.org/ 10.17485/IJST/v17i10.1910

[39] Ramya, D., Raju, R. S., Rao, J. A., Chamkha, A. J., Effects of velocity and thermal wall slip on magnetohydrodynamics (MHD) boundary layer viscous flow and heat transfer of a nanofluid over a non-linearly-stretching sheet: a numerical study, *Propul. Power Res.* **7**(2) (2018) 182–195. DOI: https://doi.org/10.1016/j.jppr.2018.04.003

[40] Rameshwaran, P., Townsend, P., Webster, M. F., Simulation of particle settling in rotating and non-rotating flows of non-Newtonian fluids, *Int. J. Numer. Methods Fluids* **26**(7) (1998) 851–874. DOI: https://doi.org/10.1002/(SICI)1097-0363(19980415)26:7<851::AID-FLD704>3.0.CO;2-4

[41] Sucharitha, G., Rashidi, M. M., Sreenadh, S., Lakshminarayana, P., Effects of magnetic field and slip on convective peristaltic flow of a non-Newtonian fluid in an inclined nonuniform porous channel with flexible walls, *J. Por. Media* **21**(10) (2018). DOI: 10.1615/JPorMedia.2018020133

[42] Ibrahim, W., Shankar, B., MHD boundary layer flow and heat transfer of a nanofluid past a permeable stretching sheet with velocity, thermal and solutal slip boundary conditions, *Comput. Fluids* **75** (2013) 1–10. DOI: https://doi.org/10.1016/j.compfluid.2013.01.014

[43] Strozzi, A., Giacopini, M., Bertocchi, E., Dini, D., Formulation of the tangential velocity slip problem in terms of variational inequalities, *Proc. Inst. Mech. Eng. Part J: J. Eng. Tribol.* **228**(10) (2014) 1122–1135. DOI: https://doi.org/10.1177/1350650114530680

[44] Ullah, Z., Alam, M. M., Elhag, S. H., Merga, F. E., Haider, I., Malik, A., Evaluation of thermal and concentration slip effects on heat and mass transmission of nanofluid over a moving wedge surface using Keller box scheme, *AIP Adv.* **14**(10) (2024). DOI:

https://doi.org/10.1063/5.0228549

[45] Vafai, K., Thiyagaraja, R., Analysis of flow and heat transfer at the interface region of a porous medium, *Int. J. Heat Mass Transf.* **30**(7) (1987) 1391–1405. https://doi.org/10.1016/0017-9310(87)90171-2

[46] Williamson, R. V., The Flow of Pseudoplastic Materials, *Ind. Eng. Chem.* **21**(11) (1929) 1108–1111. DOI: https://doi.org/10.1021/ie50239a035

[47] Zehra, I., Yousaf, M. M., Nadeem, S., Numerical solutions of Williamson fluid with pressure dependent viscosity, *Res. Phys.* **5** (2015) 20–25. DOI: https://doi.org/10.1016/j.rinp.2014.12.002